

Wall-anchored semiflexible polymer under large amplitude oscillatory shear flow

Antonio Lamura,^{1, a)} Roland G. Winkler,^{2, b)} and Gerhard Gompper^{2, c)}

¹⁾*Istituto Applicazioni Calcolo, CNR, Via Amendola 122/D, 70126 Bari, Italy*

²⁾*Theoretical Physics of Living Matter, Institute for Advanced Simulation and Institute of Biological Information Processing, Forschungszentrum Jülich, 52425 Jülich, Germany*

(Dated: 14 December 2021)

The properties of semiflexible polymers tethered by one end to an impenetrable wall and exposed to oscillatory shear flow are investigated by mesoscale simulations. A polymer, confined in two dimensions, is described by a linear bead-spring chain, and fluid interactions are incorporated by the Brownian multiparticle collision dynamics approach. At small strains, the polymers follow the applied flow field. However, at high strain, we find a strongly nonlinear response, with major conformational changes. Polymers are stretched along the flow direction and exhibit U-shaped conformations while following the flow. As a consequence of confinement in the half-space, a frequency doubling in the time-dependent polymer properties appears along the direction normal to the wall.

I. INTRODUCTION

Studies of the nonequilibrium behavior of polymer systems provide a link between their microscopic molecular characteristics and the emerging macroscopic dynamical properties^{1–6}. A major experimental breakthrough in resolving and visualizing the nonequilibrium properties of individual molecules was achieved by studies on single DNA filaments⁷, which paved the way to explore a large variety of polymer properties under flows.

From the theoretical side, several detailed computational molecular models have been considered, which enhance our understanding of molecular processes. In particular, single-polymer studies provide the opportunity to directly observe the microscopic conformational properties of individual polymers close to equilibrium or under flow conditions, thereby facilitating access to their non-equilibrium conformational properties, which are ultimately responsible for the macroscopic rheological behavior. The desire to visualize individual polymer conformations in flow, both from an experimental and simulation point of view, is strongly linked with advances in the statistical description of their properties provided by molecular theoretical models^{6,8,9}.

Semiflexible polymer-type molecular structures are omnipresent in biological systems, e.g., DNA, actin filaments, and microtubules, and their rigidity is fundamental for their functions. Indeed, actin filaments contribute with their rigidity to the mechanical properties of the cytoskeleton and the ability of DNA to pack in the genome or inside a virus capsid is controlled by its persistence length. As a consequence, the properties of semiflexible polymers have been intensively investigated^{10–17}. Here, theoretical^{9,18–21} and computational^{22–40} studies

revealed novel dynamical, conformational, and rheological properties.

The large majority of these studies focuses on three-dimensional systems, and predominantly single-polymer theoretical and simulation studies have been performed under steady shear and extensional flow in the bulk^{9,33,41}. Similarly, in experiments single DNA filaments have been considered, in particular filaments grafted on a wall by one end under steady shear, and their mechanical properties⁴² and relaxation dynamics⁴³ have been examined. Further experiments^{44,45} revealed the existence of a cyclic dynamics, which has been confirmed by simulations^{45,46}.

Polymers in two dimensions are of interest on their own. Compared to the three-dimensional case, there are two major differences. On the one hand, excluded-volume interactions are more important and, on the other hand, hydrodynamics can be neglected, specifically, in the case of strongly adsorbed polymers⁴⁷. Such systems can be realized experimentally by considering filaments strongly adsorbed onto a surface, a membrane, or at interfaces separating immiscible fluids^{47–49}. In particular, end-anchored semiflexible polymers have been considered, where the central monomer is subject to an oscillatory force, and a transition from a limit cycle to an aperiodic dynamics with increasing rigidity has been predicted theoretically⁵⁰. The dynamics of semiflexible polymers under shear has been investigated numerically and substantial stiffness-dependent conformational changes at high flow rates have been obtained⁵¹. Specifically, more flexible polymers are extended by the flow, while stiffer filaments contract. Moreover, filaments are aligned by the flow with a tumbling motion that, at high shear rates, resembles the motion of flexible polymers in three dimensions.

Theory, simulations, and experiments typically consider stationary flows in the linear viscoelastic regime. However, it is important to unravel the polymer dynamics when time-dependent flows are applied, specif-

^{a)}Corresponding author: antonio.lamura@cnr.it

^{b)}r.winkler@fz-juelich.de

^{c)}g.gompper@fz-juelich.de

ically large amplitude oscillatory shear (LAOS) flows. Such studies provide additional insight into the macroscopic polymer properties, specifically their viscoelastic behavior^{52,53}. Despite the deep interest and experimental relevance, so far very few theoretical and simulation studies have been performed under such flow conditions. In Ref.⁵⁴, the extension and migration of a chain, confined in a microchannel and subject to oscillatory pressure-driven flow, were observed. Later, Brownian dynamics studies of macromolecules under oscillatory shear flow have been performed^{55,56}. In contrast, many more LAOS experiments have been conducted^{52,53,57}. Yet, no study so far considered a single tethered semiflexible chain subject to oscillatory shear flow.

In this paper, we investigate the conformational and dynamical properties of a semiflexible polymer in two dimensions, tethered by one of its ends on a reflecting wall, in the presence of an oscillatory shear flow by mesoscale simulations. A polymer is modeled as a self-avoiding worm-like filament. Neglecting hydrodynamic interactions, the polymer is assumed to be in contact with a Brownian heat bath implemented via the Brownian version^{58,59} of the multiparticle collision dynamics approach^{59,60}. The polymer properties are characterized in terms of the strain defined as the ratio of the shear rate to the shear frequency. For low strain, the polymers behave roughly as at equilibrium. In the opposite limit of high strain, they show in each shear half-cycle average properties comparable to those at steady shear—they fully elongate and flip back and forth following the external flow. For intermediate values of strain, flipping is disfavored, and polymers may remain preferentially in a coiled state when shear changes sign without re-orientating along the instantaneous flow direction. The analysis of the amplitudes of the undulation modes suggests that polymers exhibit a flexible polymer-like behavior at larger length scales along the shear direction, despite their significant stiffness in absence of the external flow. The periodic motion of the center-of-mass displays the same frequency as the external shear along the flow direction, while frequency doubling in the normal direction appears by wall reflection, which “repels” the polymer as flow drags it from one side to the other in a cycle.

The numerical models for the polymer and the Brownian fluid are introduced in Sec. II. The results for the conformational and the dynamical behavior are presented in Sec. III. Finally, Sec. IV summarizes and discusses the main findings of this study.

II. MODEL AND METHOD

We model a filament as a linear bead-spring chain with N beads of mass M separated by bonds of length r_0 , and confined in the positive half-plane of the two dimensional space. The first bead is tethered at the origin $(0, 0)^T$ of the Cartesian reference frame, with no preferred orienta-

tion of the first bond. The beads are subjected to forces by the total potential $U = U_{bond} + U_{bend} + U_{ex} + U_w$. Bonds are described by the harmonic potential

$$U_{bond} = \frac{\kappa_h}{2} \sum_{i=1}^{N-1} (|\mathbf{r}_{i+1} - \mathbf{r}_i| - r_0)^2, \quad (1)$$

where \mathbf{r}_i denotes the position vector of the i -th bead ($i = 1, \dots, N$) and κ_h is the force constant. The stiffness of the polymer is implemented by the bending potential

$$U_{bend} = \kappa \sum_{i=1}^{N-2} (1 - \cos \varphi_i), \quad (2)$$

where κ is the bending rigidity and φ_i is the angle between two consecutive bond vectors. The filament persistence length L_p is related to κ via $L_p = 2\kappa r_0 / k_B T$, where $k_B T$ is the thermal energy, with T the temperature and k_B Boltzmann’s constant. The shifted and truncated Lennard-Jones potential

$$U_{ex} = 4\epsilon \left[\left(\frac{\sigma}{r} \right)^{12} - \left(\frac{\sigma}{r} \right)^6 + \frac{1}{4} \right] \Theta(2^{1/6}\sigma - r) \quad (3)$$

ensures the self-avoidance of non-connected beads. Here, r is the distance between two beads and $\Theta(r)$ is the Heaviside function ($\Theta(r) = 0$ for $r < 0$ and $\Theta(r) = 1$ for $r \geq 0$). Confinement in the half-plane $y > 0$ is achieved by a repulsive wall implemented via the potential

$$U_w = 4\epsilon \left[\left(\frac{\sigma_w}{y} \right)^{12} - \left(\frac{\sigma_w}{y} \right)^6 + \frac{1}{4} \right] \Theta(2^{1/6}\sigma_w - y), \quad (4)$$

where y is the distance of a bead from the wall. The dynamics of the beads is described by Newton’s equations of motion, which are integrated by the velocity-Verlet algorithm with time step Δt_p ^{61,62}.

Shear flow and thermal fluctuations are implemented by the Brownian multiparticle collision dynamics approach (B-MPC)^{58,59,63}, where hydrodynamic interactions are neglected. In this method, stochastic collisions between each bead and a number ρ of “fluid” phantom particles of mass m mimic interactions of a fluid volume surrounding a bead. The moment of a phantom particle is Maxwellian distributed, with variance $mk_B T$ and mean $(m\dot{\gamma}y \sin(2\pi t/T), 0)^T$ at time t in the presence of the oscillating shear flow of shear rate $\dot{\gamma}$, period T , and orientation along the x -axis. The collision process itself is implemented via the stochastic rotation dynamics (SRD) variant of the MPC method^{59,64,65}. Here, the relative velocity of a bead, with respect to the center-of-mass velocity of the bead and its related phantom particles, is rotated in the xy -plane by a fixed angle $\pm\alpha$ of uniformly distributed sign. Collisions occur at time intervals Δt , where $\Delta t > \Delta t_p$.

Simulations are performed for the parameters: $\alpha = 130^\circ$, $\Delta t = 0.1t_u$, with the time unit $t_u = \sqrt{mr_0^2/(k_B T)}$, $M = \rho m$, $\rho = 5$, $\kappa_h r_0^2/(k_B T) = 4 \times 10^3$, $\epsilon/(k_B T) = 1$, $\sigma = r_0$, $\sigma_w = r_0/2$, $N = 101$, and $\Delta t_p = 10^{-2}\Delta t$. The value of κ_h ensures the length $L = 100r_0$ of the polymer within 1% for all systems and flow conditions.

III. RESULTS

We study semiflexible polymers with the persistence lengths $L_p/L = 0.5$ and 2. B-MPC simulations of free filaments yield the end-to-end vector relaxation times $\tau_r \simeq (1.9, 3.9) \times 10^6 t_u$ ⁵¹. The tethered polymers are initialized with beads aligned along the y -direction, and are equilibrated up to $5 \times 10^6 t_u$. Subsequently, data are collected up to the longest simulated time $10^8 t_u$ and averaged over half-periods with positive shear flow. The flow is characterized in terms of the Weissenberg number $Wi = \tau_r \dot{\gamma}$ and the Deborah number $De = \tau_r \omega$, where $\omega = 2\pi/T$ is the shear frequency. Since in oscillatory flow the strain in a half-cycle is proportional to $\dot{\gamma}/\omega = Wi/De$, averages will be characterized as function of this ratio in the following. The shear rate is varied the range $0 \leq Wi \lesssim 10^3$, while the frequency is altered such that $0.1 \leq Wi/De \leq 100$.

A. Conformational properties

We characterize the filament conformational properties by the end-to-end vector $\mathbf{R}_e = \mathbf{r}_N - \mathbf{r}_1$. The oscillatory shear implies a cyclic dynamics of filament collapse, stretching, and alignment along the flow direction (see movies movie1.mp4, movie2.mp4, movie3.mp4, and movie4.mp4 in supplementary material.).

1. Filament stretching

Stretching along the flow direction is characterized by the maximum extension $R_{ex,max}$ of the polymer along the x -axis in a cycle, or, equivalently, by the average deficit length-ratio $\varepsilon = 1 - \langle R_{ex,max} \rangle / L$, where the average is performed over periods.

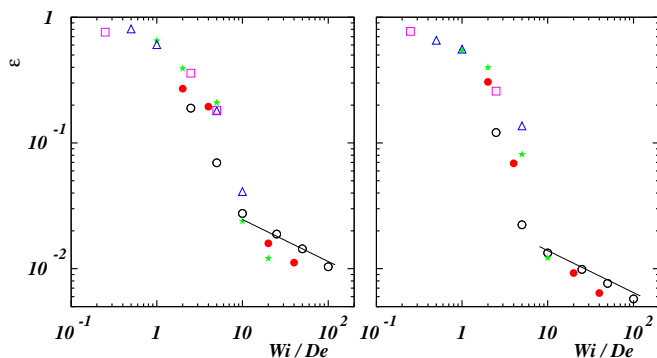


FIG. 1. Mean deficit length-ratio ε as a function of the strain Wi/De for $L_p/L = 0.5$ (left), 2 (right) and $De = 10$ (○, black), 25 (●, red), 50 (★, green), 100 (△, blue), and 200 (□, magenta). The slope of the full lines is $-1/3$.

Figure 1 displays ε as a function of the strain Wi/De . The data for the various De nearly collapse when plot-

ted as function of Wi/De , a feature applying to other quantities too. Three regimes can be identified, which we will denote as low- ($Wi/De \lesssim 1$), intermediate- ($1 \lesssim Wi/De \lesssim 10$), and high-strain regime ($Wi/De \gtrsim 10$). In the low-strain regime, either the shear rate or/and the period are so small that the shear is hardly able to deform the polymer compared to the equilibrium value. With increasing strain beyond unity, the deficit length decreases very rapidly and for $Wi/De > 10$ a power-law regime seems to appear, with an exponent of $-1/3$ for $De = 10$. This exponent is consistent with experimental results on tethered semiflexible DNA molecules under steady shear⁶⁶. The high-strain regime corresponds to high values either of the shear rate or the shear period, implying a large polymer stretching ($\varepsilon \lesssim 10^{-2}$), and the approximations of Ref.⁶⁶ in the derivation of shear-rate dependence apply. For $De > 10$, there seem to be some deviations from the power law $-1/3$, or the power-law regime has not yet been reached; a detailed analysis is hampered by necessary very large shear rates. Noteworthy, stiffer polymers are stronger stretched than flexible ones.

2. Height above wall

Confinement to the positive semi-space breaks spatial symmetry and leads to a geometry-induced polymer stretching normal to the wall. The dependence of the height above the wall, defined as the average distance $\langle y_N \rangle$ of bead N from the wall, on strain is depicted in Fig. 2.

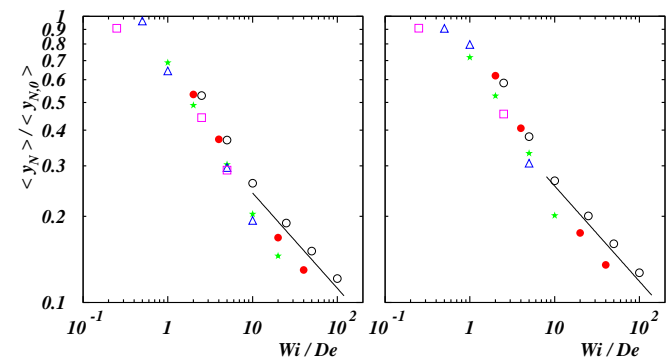


FIG. 2. Mean polymer height above wall as a function of the strain Wi/De for $L_p/L = 0.5$ (left), 2 (right), and $De = 10$ (○, black), 25 (●, red), 50 (★, green), 100 (△, blue), and 200 (□, magenta). The solid lines indicate the slope $-1/3$. $\langle y_{N,0} \rangle$ is the mean polymer height at equilibrium.

The height decreases with increasing strain according to the power-law $\langle y_N \rangle \sim (Wi/De)^{-1/3}$ for high strain, independent of the considered stiffness. The range of the scaling regime roughly coincides with that in Fig. 1 for the deficit length. Moreover, our simulations yield the dependence $\langle y_N^2 \rangle \sim (Wi/De)^{-2/3} \sim \langle y_N \rangle^2$ in the high

Wi/De regime. This dependence agrees with the scaling prediction for the fluctuations normal to a wall of a free-draining semiflexible polymers under shear flow⁶⁶.

3. Polymer deformation

More detailed insight onto the polymer deformation is gained by the distribution function of the end-to-end vector $R_e = |\mathbf{R}_e|$ (see Fig. 3). In the absence of shear, the distribution function exhibits a single peak at $R_e/L \simeq 1$ for $L_p/L = 2$ corresponding to a fully elongated configuration. With decreasing persistence length, the distribution broadens and the peak moves to $R_e/L \simeq 0.87$. For the stiffer chain at small strain, $Wi/De = 2.5$, the conformations are already substantially affected by shear, and R_e values over a broad range, $0.3 \lesssim |R_e/L| \lesssim 0.85$, are nearly equally probable. This range broadens with decreasing De at fixed Wi , the probabilities in the plateau-like regime decrease, and a peak appears in the vicinity of full stretching. The latter indicates an increasing probability of strongly-stretched polymers. At the same time, $P(R_e)$ decreases at smaller end-to-end vectors. We obtain approximately the same distribution functions for the more flexible polymer.

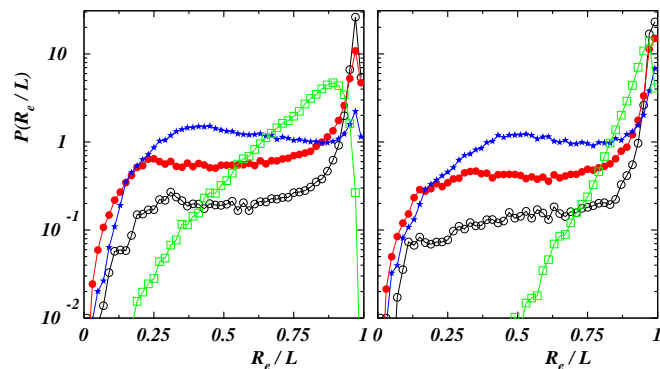


FIG. 3. Probability distribution function of the polymer end-to-end distance $|\mathbf{R}_e|$ for $L_p/L = 0.5$ (left) and 2 (right), and the Weissenberg number $Wi = 0$ (\square , green) as well as $Wi = 500$ for $De = 10$ (\circ , black), 50 (\bullet , red), 200 (\star , blue).

The variations of the distribution function with De affect the average end-to-end vector R_e . Associated with the overall decrease of the distribution function by a change of Wi/De from zero to $Wi/De = 2.5$, is a small drop of the average mean end-to-end distance, $\langle R_e \rangle$. A further increase of Wi/De implies a monotonic swelling of $\langle R_e \rangle$. At the same time, $\langle (R_e - \langle R_e \rangle)^2 \rangle$ swells first with increasing strain, reaches a maximum at $Wi/De \approx 8$, and decreases then by a power-law with the exponent $-1/3$.

B. Dynamical properties

Figure 4 displays conformations of polymers during one period. At high strain, a polymer flips back and forth

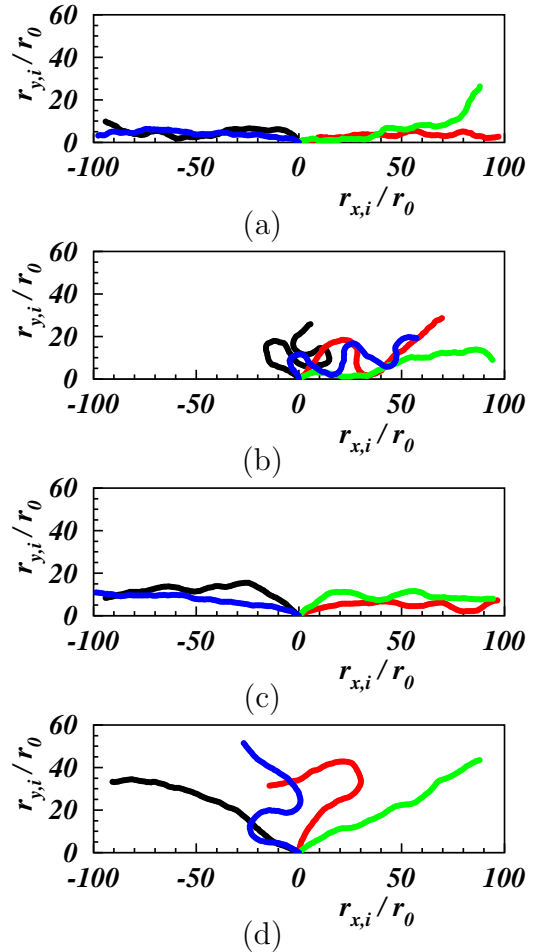


FIG. 4. Polymer conformations at the times $t/T = 1, 1.25, 1.5, 1.75$ (black, red, green, and blue lines, respectively) after equilibration for $L_p/L = 0.5$ ((a), (b)) and $L_p/L = 2$ ((c), (d)), $Wi = 500$, and $De = 10$ ((a), (c)) and 200 ((b), (d)). (See movies movie1.mp4 for the case (a), movie2.mp4 for the case (c), movie3.mp4 for the case (b), and movie4.mp4 for the case (d) in supplementary material.)

following the applied shear. However, the flipping mechanism strongly depends on the interplay of shear and bending rigidity. In the case of a more flexible polymer, the polymer recoils after the flow changes sign, then flips and elongates (see supplementary movie movie1.mp4). In contrast, the stiffer polymer bends, assumes a U-shaped conformation during flipping, and finally elongates (see the supplementary movie movie2.mp4). Smaller strain disfavors chain flip when the flow changes sign. Here, a polymer remains coiled without flipping (see Fig. 4 (b) and the supplementary movie movie3.mp4), and, consequently, remains essentially in the positive half-space $x > 0$. This behavior is also observed for higher bend-

ing stiffness. In the latter case, however, the chain flip occurs more frequently than in the flexible case with the polymer recoiling and reorienting (see Fig. 4 (d) and the supplementary movie movie4.mp4).

The described mechanism of chain flipping is supported by the probability distribution functions $P(\Phi)$ of the inclination angle Φ , which is defined as the angle between the polymer center-of-mass position vector and the flow direction (Fig. 5). For large strain, the polymers

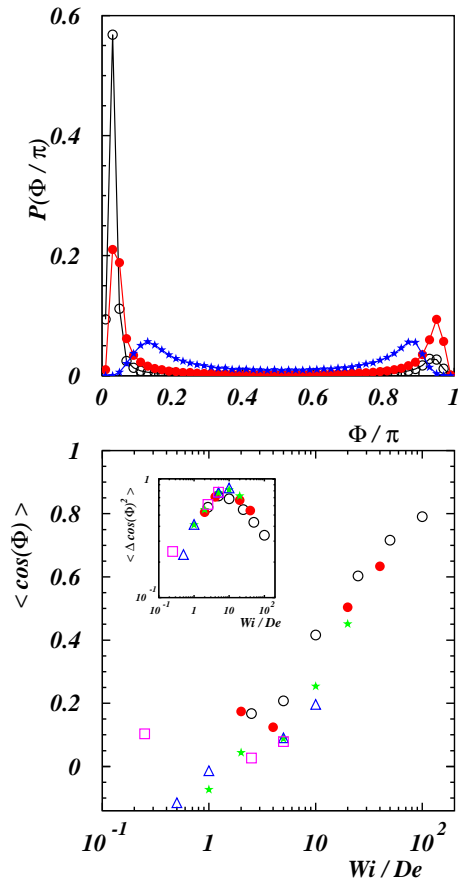


FIG. 5. (Top) Probability distribution function of the polymer inclination angle Φ based on data from positive half-cycle for $L_p/L = 0.5$, $De = 10$ (\circ , black), 50 (\bullet , red), 200 (\star , blue), and $Wi = 500$. The distribution functions for negative half-cycle are mirror symmetric with respect to $\Phi/\pi = 1/2$. (Bottom) Average of $\cos \Phi$ as a function of the strain Wi/De for $L_p/L = 0.5$ and $De = 10$ (\circ , black), 25 (\bullet , red), 50 (\star , green), 100 (\triangle , blue), and 200 (\square , magenta). The inset shows the variance $\langle (\cos \Phi - \langle \cos \Phi \rangle)^2 \rangle$ as a function of Wi/De for $L_p/L = 0.5$ and $De = 10$ (\circ , black), 25 (\bullet , red), 50 (\star , green), 100 (\triangle , blue), and 200 (\square , magenta).

spend most of their time aligned with the flow direction (the main peak is located at $\Phi < \pi/2$) during the positive half-cycle of the shear oscillation (Fig. 5 (left)), and opposite to the flow direction (the main peak is at $\Phi > \pi/2$) during the negative half-cycle of the shear oscillation (the distribution functions for the negative half-cycle are mir-

ror symmetric with respect to $\Phi = \pi/2$). This suggests that for high values of the strain the inclination angle and the shear flow are of the same sign before the shear flow changes sign. Interestingly, for the lowest considered value $Wi/De = 2.5$, the distribution function $P(\Phi)$ for the positive and negative half-cycles are indistinguishable for the considered persistence lengths— $P(\Phi)$ shows two broad peaks of comparable height symmetric with respect to the shear direction ($\Phi = \pi/2$). This indicates that polymers can either flip or keep their orientation with equal probability, when the shear rate changes sign.

The average, $\langle \cos \Phi \rangle$ (Fig. 5 (right)), of the inclination angle depends weakly on shear and increases logarithmically, $\langle \cos \Phi \rangle \sim \log(Wi/De)$, on strain, while its variance has a maximum for intermediate values of strain.

1. Center-of-mass motion

Figure 6 illustrates the time dependence of the center-of-mass, $\mathbf{r}_{cm} = (x_{cm}, y_{cm})^T$, during three periods for $L_p/L = 0.5$. For the highest considered strain $Wi/De = 50$ (Fig. 6(a)), x_{cm} exhibits a nearly in-phase periodic motion with a small phase shift θ , and the dynamics is apparently no longer harmonic. The component y_{cm} shows very narrow peaks whenever x_{cm} changes sign and becomes very small as soon as the polymer is stretched. Remarkably, y_{cm} exhibits frequency doubling. We like to stress that the frequency doubling is independent of the considered quantity used to characterize the center-of-mass motion. Specifically, we considered the time dependence of the inclination angle Φ and that of the distance $R_{cm} = \sqrt{x_{cm}^2 + y_{cm}^2}$. While Φ exhibits the same frequency as the applied flow, R_{cm} shows frequency doubling. With decreasing Wi/De , the motion is still periodic and becomes more harmonic with a larger phase shift (Fig. 6(b)). The y_{cm} peaks are now broader and their amplitude decreases. Finally, for the smallest value $Wi/De = 2.5$ (Fig. 6(c)), x_{cm} partially follows the external flow with a reduced amplitude which is no longer symmetric with respect to $x = 0$ due to entropic effects, and the magnitude of the angle θ further increases. The time sequence of y_{cm} indicates that the polymer is no longer fully elongated along the wall when the flow reaches its extreme values. The peaks are very broad and no clear indication of a frequency doubling can be observed, since the amplitude of y_{cm} is significantly reduced. The comparable data for $L_p/L = 2$ show no appreciable differences. In order to evaluate the phase shift θ , the values of x_{cm} are fitted to the function $A \sin(\omega t + \theta)$, where A and θ are fitting parameters. The values of θ are in the range $(-\pi/2, 0)$ and appear to be independent on the persistence length (Fig. 7). The extracted dependence on Wi/De can well be described by the function $\theta = \text{arccot}(-aWi/De)$, with $a = 0.054$.

Further evidence of the discussed frequency doubling is obtained by the autocorrelation functions of the Cartesian center-of-mass coordinates (Fig. 8). Consistent with

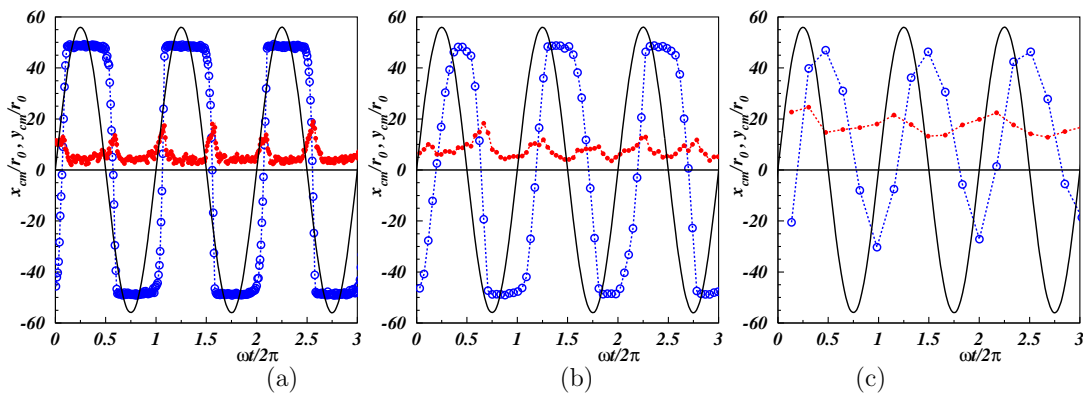


FIG. 6. Time dependence of the polymer center-of-mass position along the flow (\circ , blue), x_{cm} , and the gradient (\bullet , red), y_{cm} , directions for $L_p/L = 0.5$, $Wi = 500$, and $De = 10$ (a), 50(b), and 200(c). The black lines indicate the externally applied shear flow with arbitrary amplitude, and the dashed lines are guides for the eye.

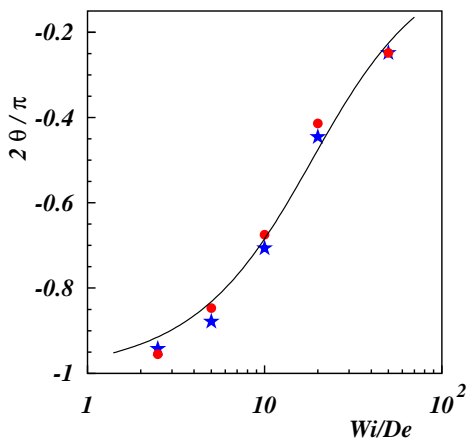


FIG. 7. Dependence of the phase shift θ on the strain Wi/De for $L_p/L = 0.5$ (\star , blue) and 2 (\bullet , red), with $Wi = 500$. The full line represents the fitted functional dependence $2 \arccot(-0.054Wi/De)/\pi$.

Fig. 6, the correlation functions display a periodic motion. The x_{cm} -component reveals the same frequency as the external flow. More importantly, the y_{cm} -component clearly shows frequency doubling for $Wi/De \gtrsim 10$. The wall at $y = 0$ reflects the polymer every time the flow moves the polymer from one side to the other. This process occurs twice in every flow cycle causing the observed frequency doubling in the dynamics along the y axis.

C. Internal polymer dynamics

The snapshots of Fig. 4 reveal strong polymer conformational changes during oscillation cycles. We characterize the appearing internal polymer dynamics by the

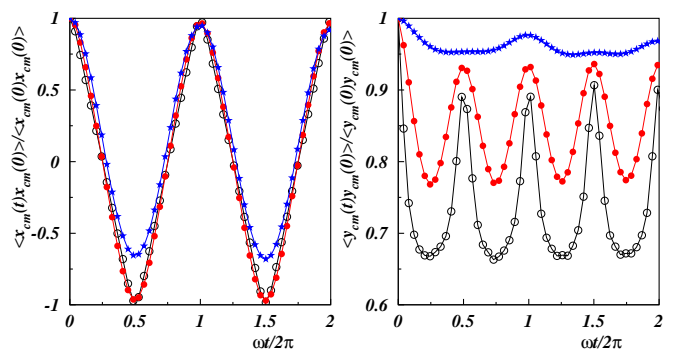


FIG. 8. Time auto-correlations of the center-of-mass x_{cm} (left) and y_{cm} (right) Cartesian coordinates for $L_p/L = 2$, $Wi = 500$, and $De = 10$ (\circ , black), 50 (\bullet , red), 200 (\star , blue).

normal mode expansion

$$\mathbf{r}_i = \sum_{n=1}^{N-1} \mathbf{A}_n(t) \sin[q_n(i-1)], \quad i = 1, \dots, N, \quad (5)$$

with the wave vectors $q_n = (n-1/2)\pi/(N-1)$ ($n = 1, \dots, N-1$). The normal mode amplitudes $\mathbf{A}_n(t) = (A_{x,n}(t), A_{y,n}(t))^T$ are given by

$$A_{x,n} = \frac{2}{N-1} \sum_{i=1}^N r_{x,i} \sin[q_n(i-1)], \quad (6)$$

$$A_{y,n} = \frac{2}{N-1} \sum_{i=1}^N r_{y,i} \sin[q_n(i-1)]. \quad (7)$$

The dependence of the variance of the mode amplitudes $\langle \delta \mathbf{A}_n^2 \rangle = \langle (\mathbf{A}_n - \langle \mathbf{A}_n \rangle)^2 \rangle$ on the mode number is illustrated in Fig. 9 for the stiffer polymer. Evidently, the variances of $A_{x,n}$ and $A_{y,n}$ are distinctly different for the considered strains. In the absence of shear, both components of the mode amplitudes exhibit the mode

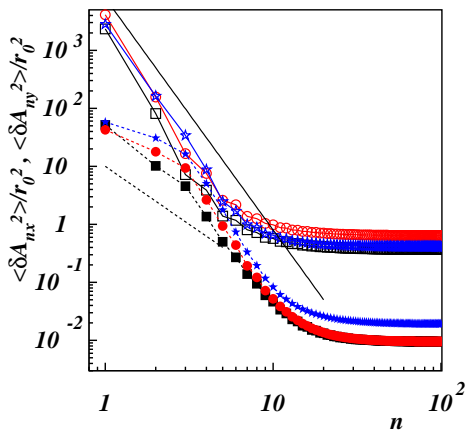


FIG. 9. Variance of the mode amplitudes $A_{x,n}$ (empty symbols connected by full lines) and $A_{y,n}$ (filled symbols connected by dashed lines) as functions of mode number n for $L_p/L = 2$ with $Wi = 500$ and $De = 10$ (\square , black), 50 (\circ , red), 200 (\star , blue). The slopes of full and dashed lines are -4 and -2 , respectively.

number dependence n^{-4} , in accordance with the semiflexible character of the considered polymers^{67,68}. Note that the plateau for large mode numbers is a consequence of the discreteness of the polymer with a finite number of modes. Along the flow direction, the n^{-4} dependence persists even under shear due to the strong polymer stretching. However, we observe a pronounced strain effects on $A_{y,n}$ for small mode numbers $3 \leq n \leq 5$. The indicated dependence n^{-2} , typical for flexible polymers^{67,69,70}, suggests that the polymer acquires a flexible polymer-like behavior on larger length scales, with a crossover to semiflexibility, n^{-4} dependence, on smaller scale, along the gradient direction. A similar behavior is found for the more flexible chain.

The dynamics of the mode amplitudes with $n = 1, 2$ is analyzed in terms of the mode-autocorrelation functions $\langle A_{x,n}(t)A_{x,n}(0) \rangle$ and $\langle A_{y,n}(t)A_{y,n}(0) \rangle$. Results for various strains and the persistence length $L_p/L = 2$ are presented in Fig. 10. The simulation data are fitted by the function

$$f(t) = A [\exp(-\gamma t/T) - 1] + B [\cos(\Omega \omega t) - 1] + C [\cos(2\Omega \omega t) - 1] + 1, \quad (8)$$

where the dimensionless factors γ and Ω characterizes the relaxation time and possible variations of the frequency with respect to the imposed ω , respectively. The correlation functions for $De = 50$ and $De = 200$ are well fitted by Eq. (8), while data for $De = 10$ do not allow for a suitable fitting. The factor γ of the x component decreases with increasing mode number, n , revealing a faster relaxation on larger length-scales along the flow direction. Thereby, γ depends on De and is larger for $De = 200$. It increases with increasing ratio Wi/De , reflecting the strong dependence of the relaxation process on the external field.

At equilibrium, the variance $\langle \delta A_n^2 \rangle$ of the amplitudes is determined by the polymer relaxation times⁷⁰. The mode-number dependence of γ is inconsistent with that of $\langle \delta A_n^2 \rangle$ (Fig. 9), which indicates a strong influence of the external field on the time dependence of the internal relaxation process. Along the y direction, γ is approximately constant at fixed strain, indicating that the chain relaxation time does not vary significantly on large scales along the shear direction.

The factor Ω is close to unity and oscillations occur with the external frequency. For both, the x and y components, the term with 2ω contributes to the oscillations of the correlation function, i.e., the observed frequency doubling found for the center-of-mass motion is also reflected in the internal dynamics.

IV. CONCLUSIONS

We have analyzed the conformational and dynamical properties of semiflexible polymers tethered at an impenetrable wall under oscillatory shear flow. We identify three different regimes in terms of polymer deformation as a function of strain. At small strain, $Wi/De \lesssim 1$, the polymer structures are close to the equilibrium conformations and they are hardly affected by flow. For intermediate strain, $1 < Wi/De < 10$, the polymer is gradually stretched and its end-to-end distance increases logarithmically. Above $Wi/De \gtrsim 10$, the deficit length exhibits a power-law decrease with increasing strain, in agreement with experimental results under steady shear flow^{44,66}.

The polymer conformations are tightly coupled with their dynamics. At high strain, the polymers follow the external oscillations of the flow with a small phase shift, and are strongly stretched and aligned with the wall. The polymer dynamics is far less enslaved by the flow field for intermediate strains, which is reflected by a larger phase difference between the flow-induced polymer structures and the external flow. Most importantly, this allows for more swollen polymer-like conformations and a higher polymer density above the wall.

As might be expected for the considered geometry, conformational properties normal to the wall exhibit frequency doubling compared to the external frequency ω , for example, the autocorrelation function of the y -center-of-mass coordinate. While the properties along the x direction are typically symmetric in terms of positive and negative values, those along y are not and only positive values are possible. Hence, positive y values correspond to positive and negative x values, which determines the frequency doubling.

In absence of chirality and torsion, we expect semiflexible polymers in three dimensions to exhibit similar features in terms of conformational changes. This is reflected in the similarity of our results with experiments of DNA molecules tethered to a wall under shear flow⁶⁶. Hydrodynamic interactions influence the polymer

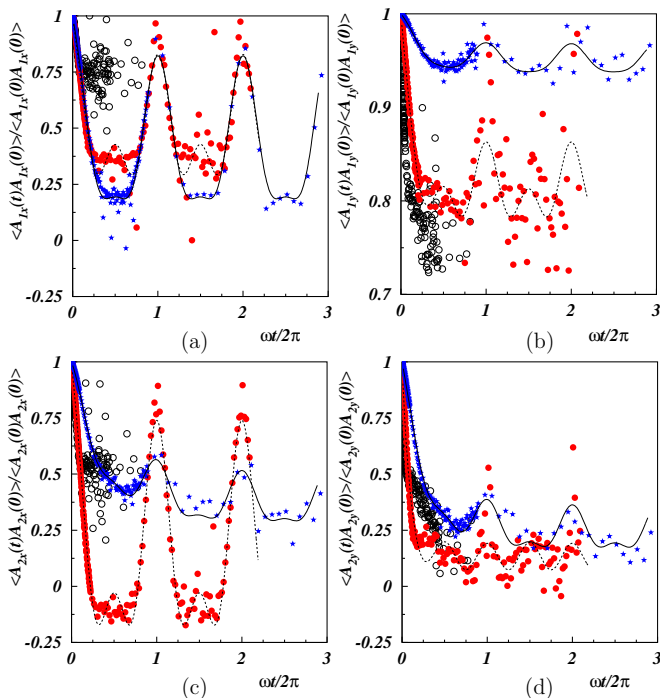


FIG. 10. Autocorrelation function of the mode amplitudes for the modes $n = 1$ along the (a) x - and (b) y -direction as well as for $n = 2$ along the (c) x - and (d) y -direction as a function of time with $L_p/L = 2$, $Wi = 500$, and $De = 10$ (\circ , black), 50 (\bullet , red), 200 (\star , blue). The black dotted and solid lines are fits of Eq. (8) to the data for $De = 50$ and $De = 200$, respectively.

dynamics, however, the extent depends on their stiffness. As far as semiflexible polymers are concerned, hydrodynamic interactions are of minor importance, so that the observed conformational and dynamical features will also be present for polymers embedded in a fluid even in three dimensions. Hydrodynamic interactions are expected to more severely affect the dynamics of flexible polymers. They are again weak for rather stretched conformations⁶⁶, but can dominate the dynamics in the coiled state and accelerate the polymer motion. In particular, this affects the internal dynamics along the y direction, with a rather Zimm- than Rouse-like mode dependence of the relaxation times on larger length scales⁷⁰.

Our simulations provide valuable insight into the properties of polymers exposed to oscillatory flows. Specifically, we demonstrate that such simulations are feasible for experimentally relevant parameters. Our studies are a first step only toward systematic investigations of polymer properties under oscillatory shear and we hope that they will prompt further simulations along that line.

SUPPLEMENTARY MATERIAL

The supplementary movies show the animations of the polymer dynamics over two shear periods for the cases reported in Fig. 4. Movie 1 is relative to the case with $L_p/L = 0.5$, $Wi = 500$, $De = 10$, movie 2 is relative to the case with $L_p/L = 2$, $Wi = 500$, $De = 10$, movie 3 is relative to the case with $L_p/L = 0.5$, $Wi = 500$, $De = 200$, and movie 4 is relative to the case with $L_p/L = 2$, $Wi = 500$, $De = 200$.

ACKNOWLEDGMENTS

A. L. thanks G. G., R. G. W., and co-workers for their hospitality during the stay at the Forschungszentrum Jülich and acknowledges support from the DAAD through the “Research Stays for University Academics and Scientists” program.

DATA AVAILABILITY STATEMENT

The data that support the findings of this study are available from the corresponding author upon reasonable request.

- ¹R. B. Bird, R. C. Armstrong, and O. Hassager, *Dynamics of Polymer Liquids*, Vol. 1 (John Wiley & Sons, New York, 1987).
- ²R. G. Larson, *The Structure and Rheology of Complex Fluids* (Oxford University Press, New York, 1999).
- ³M. Rubinstein and R. C. Colby, *Polymer Physics* (Oxford University Press, Oxford, 2003).
- ⁴R. G. Larson and P. S. Desai, “Modeling the rheology of polymer melts and solutions,” *Ann. Rev. Fluid Mech.* **47**, 47 (2015).
- ⁵M. T. Shaw and W. J. MacKnight, *Introduction to polymer viscoelasticity* (John Wiley & Sons, 2018).
- ⁶C. M. Schroeder, *J. Rheol.* **62**, 371 (2018).
- ⁷T. T. Perkins, D. E. Smith, R. G. Larson, and S. Chu, *Science* **268**, 83 (1995).
- ⁸R. G. Winkler, “Semiflexible polymers in shear flow,” *Phys. Rev. Lett.* **97**, 128301 (2006).
- ⁹R. G. Winkler, “Conformational and rheological properties of semiflexible polymers in shear flow,” *J. Chem. Phys.* **133**, 164905 (2010).
- ¹⁰J. Wilhelm and E. Frey, “Radial distribution function of semiflexible polymers,” *Phys. Rev. Lett.* **77**, 2581 (1996).
- ¹¹R. Götter, K. Kroy, E. Frey, M. Bärmann, and E. Sackmann, *Macromolecules* **29**, 30 (1996).
- ¹²L. Harnau, R. G. Winkler, and P. Reineker, “Dynamic structure factor of semiflexible macromolecules in dilute solution,” *J. Chem. Phys.* **104**, 6355 (1996).
- ¹³R. Everaers, F. Jülicher, A. Ajdari, and A. C. Maggs, “Dynamic fluctuations of semiflexible filaments,” *Phys. Rev. Lett.* **82**, 3717 (1999).
- ¹⁴J. Samuel and S. Sinha, “Elasticity of semiflexible polymers,” *Phys. Rev. E* **66**, 050801 (2002).
- ¹⁵L. Le Goff, O. Hallatschek, E. Frey, and F. Amblard, “Tracer studies on f-actin fluctuations,” *Phys. Rev. Lett.* **89**, 258101 (2002).
- ¹⁶R. G. Winkler, “Deformation of semiflexible chains,” *J. Chem. Phys.* **118**, 2919 (2003).
- ¹⁷E. P. Petrov, T. Ohrt, R. G. Winkler, and P. Schuille, “Diffusion and segmental dynamics of double-stranded DNA,” *Phys. Rev. Lett.* **97**, 258101 (2006).

- ¹⁸R. B. Bird, C. F. Curtiss, R. C. Armstrong, and O. Hassager, *Dynamics of Polymer Liquids*, Vol. 2 (John Wiley & Sons, New York, 1987).
- ¹⁹H. C. Öttinger, *Stochastic Processes in Polymeric Fluids* (Springer, Berlin, 1996).
- ²⁰R. G. Winkler, “Semiflexible polymers in shear flow,” *Phys. Rev. Lett.* **97**, 128301 (2006).
- ²¹T. Munk, O. Hallatschek, C. H. Wiggins, and E. Frey, “Dynamics of semiflexible polymers in a flow field,” *Phys. Rev. E* **74**, 041911 (2006).
- ²²J. S. Hur and E. S. G. Shaqfeh, “Brownian dynamics simulations of single DNA molecules in shear flow,” *J. Rheol.* **44**, 713 (2000).
- ²³R. M. Jendrejack, J. J. de Pablo, and M. D. Graham, “Stochastic simulations of dna in flow: Dynamics and the effects of hydrodynamic interactions,” *J. Chem. Phys.* **116**, 7752 (2002).
- ²⁴C.-C. Hsieh and R. G. Larson, “Modelling hydrodynamic interaction in Brownian dynamics: Simulation of extensional and shear flows of dilute solutions of high molecular weight polystyrene,” *J. Rheol.* **48**, 995 (2004).
- ²⁵S. Liu, B. Ashok, and M. Muthukumar, “Brownian dynamics simulations of beadrod-chain in simple shear flow and elongational flow,” *Polymer* **45**, 1383 (2004).
- ²⁶A. Celani, A. Puliafito, and K. Turitsyn, “Polymers in linear shear flow: A numerical study,” *Europhys. Lett.* **70**, 464 (2005).
- ²⁷J. F. Ryder and J. M. Yeomans, “Shear thinning in dilute polymer solutions,” *J. Chem. Phys.* **125**, 194906 (2006).
- ²⁸M. Ripoll, R. G. Winkler, and G. Gompper, “Star polymers in shear flow,” *Phys. Rev. Lett.* **96**, 188302 (2006).
- ²⁹C. Sendner and R. R. Netz, *EPL* **81**, 54006 (2008).
- ³⁰G.-L. He, R. Messina, H. Löwen, A. Kiriy, V. Bocharova, and M. Stamm, “Shear-induced stretching of adsorbed polymer chains,” *Soft Matter* **5**, 3014 (2009).
- ³¹Y. Zhang, A. Donev, T. Weisgraber, B. J. Alder, M. G. Graham, and J. J. de Pablo, “Tethered dna dynamics in shear flow,” *J. Chem. Phys.* **130**, 234902 (2009).
- ³²C.-C. Huang, R. G. Winkler, G. Sutmann, and G. Gompper, “Semidilute polymer solutions at equilibrium and under shear flow,” *Macromolecules* **43**, 10107 (2010).
- ³³C.-C. Huang, G. Sutmann, G. Gompper, and R. G. Winkler, “Tumbling of polymers in semidilute solution under shear flow,” *EPL* **93**, 54004 (2011).
- ³⁴C.-C. Huang, G. Gompper, and R. G. Winkler, “Nonequilibrium relaxation and tumbling times of polymers in semidilute solution,” *J. Phys.: Condens. Matter* **24**, 284131 (2012).
- ³⁵P. S. Lang, B. Obermayer, and E. Frey, *Phys. Rev. E* **89**, 022606 (2014).
- ³⁶A. Nikoubashman and M. P. Howard, *Macromolecules* **50**, 8279 (2017).
- ³⁷X. Kong, Y. Han, W. Chen, F. Cui, and Y. Li, *Soft Matter* **15**, 6353 (2019).
- ³⁸A. Romo-Uribe, *J. Appl. Polym. Sci.* **138**, 49712 (2021).
- ³⁹A. Shee, N. Gupta, A. Chaudhuri, and D. Chaudhuri, *Soft Matter* **17**, 2120 (2021).
- ⁴⁰A. Nikoubashman, *J. Chem. Phys.* **154**, 090901 (2021).
- ⁴¹E. S. G. Shaqfeh, *J. Non-Newtonian Fluid Mech.* **130**, 1 (2005).
- ⁴²S. B. Smith, L. Finzi, and C. Bustamante, *Science* **258**, 1122 (1992).
- ⁴³T. T. Perkins, S. R. Quake, D. E. Smith, and S. Chu, *Science* **264**, 822 (1994).
- ⁴⁴P. S. Doyle, B. Ladoux, and J.-L. Viovy, “Dynamics of a tethered polymer in shear flow,” *Phys. Rev. Lett.* **84**, 4769 (2000).
- ⁴⁵C. A. Lueth and E. S. G. Shaqfeh, *Macromolecules* **42**, 9170 (2009).
- ⁴⁶R. Delgado-Buscalioni, “Cyclic motion of a grafted polymer under shear flow,” *Phys. Rev. Lett.* **96**, 088303 (2006).
- ⁴⁷B. Maier, U. Seifert, and J. O. Rädler, *Europhys. Lett.* **60**, 622 (2002).
- ⁴⁸A. G. Cherstvy and E. P. Petrov, “Modeling dna condensation on freestanding cationic lipid membranes,” *Phys. Chem. Chem. Phys.* **16**, 2020 (2014).
- ⁴⁹C. Herold, P. Schwille, and E. P. Petrov, “Dna condensation at freestanding cationic lipid bilayers,” *Phys. Rev. Lett.* **104**, 148102 (2010).
- ⁵⁰A. K. Chattopadhyay and D. Marenduzzo, *Phys. Rev. Lett.* **98**, 088101 (2007).
- ⁵¹A. Lamura and R. G. Winkler, “Semiflexible polymers under external fields confined to two dimensions,” *J. Chem. Phys.* **137**, 244909 (2012).
- ⁵²K. Hyun, M. Wilhelm, C. O. Klein, K. S. Cho, J. G. Nam, K. H. Ahn, S. J. Lee, R. H. Ewoldt, and G. H. McKinley, “A review of nonlinear oscillatory shear tests: Analysis and application of large amplitude oscillatory shear (LAOS),” *Prog. Poly. Sci.* **36**, 1697 (2011).
- ⁵³S. Rogers, “Large amplitude oscillatory shear: Simple to describe, hard to interpret,” *Physics Today* **71**, 34 (2018).
- ⁵⁴Y.-L. Chen, M. D. Graham, J. J. de Pablo, K. Jo, and D. C. Schwartz, *Macromolecules* **38**, 6680 (2005).
- ⁵⁵D. G. Thomas, R. J. DePuit, and B. Khomami, *J. Rheol.* **53**, 275 (2009).
- ⁵⁶A. Lamura and R. G. Winkler, “Tethered semiflexible polymer under large amplitude oscillatory shear,” *Polymers* **11**, 737 (2019).
- ⁵⁷Y. Zhou and C. M. Schroeder, *Phys. Rev. Fluids* **1**, 053301 (2016).
- ⁵⁸M. Ripoll, R. G. Winkler, and G. Gompper, “Hydrodynamic screening of star polymers in shear flow,” *Eur. Phys. J. E* **23**, 349 (2007).
- ⁵⁹G. Gompper, T. Ihle, D. M. Kroll, and R. G. Winkler, “Multi-particle collision dynamics: A particle-based mesoscale simulation approach to the hydrodynamics of complex fluids,” *Adv. Polym. Sci.* **221**, 1 (2009).
- ⁶⁰R. Kapral, “Multiparticle collision dynamics: Simulations of complex systems on mesoscale,” *Adv. Chem. Phys.* **140**, 89 (2008).
- ⁶¹W. C. Swope, H. C. Andersen, P. H. Berens, and K. R. Wilson, “A computer simulation method for the calculation of equilibrium constants for the formation of physical clusters of molecules: Application to small water clusters,” *J. Chem. Phys.* **76**, 637 (1982).
- ⁶²M. P. Allen and D. J. Tildesley, *Computer Simulation of Liquids* (Clarendon Press, Oxford, 1987).
- ⁶³A. Malevanets and J. M. Yeomans, “Dynamics of short polymer chains in solution,” *Europhys. Lett.* **52**, 231–237 (2000).
- ⁶⁴T. Ihle and D. M. Kroll, “Stochastic rotation dynamics: A Galilean-invariant mesoscopic model for fluid flow,” *Phys. Rev. E* **63**, 020201(R) (2001).
- ⁶⁵A. Lamura, G. Gompper, T. Ihle, and D. M. Kroll, “Multiparticle collision dynamics: Flow around a circular and a square cylinder,” *Europhys. Lett.* **56**, 319–325 (2001).
- ⁶⁶B. Ladoux and P. S. Doyle, “Stretching tethered dna chains in shear flow,” *Europhys. Lett.* **52**, 511 (2000).
- ⁶⁷L. Harnau, R. G. Winkler, and P. Reineker, *J. Chem. Phys.* **102**, 7750 (1995).
- ⁶⁸S. R. Aragón and R. Pecora, *Macromolecules* **18**, 1868 (1985).
- ⁶⁹P. E. Rouse, *J. Chem. Phys.* **21**, 1272 (1953).
- ⁷⁰M. Doi and S. F. Edwards, *The Theory of Polymer Dynamics* (Clarendon Press, Oxford, 1986).